Technische Mechanik, Band 24, Heft 3-4, (2004), 242-253
Manuskripteingang: 19. April 2004

High-Order Sub-Harmonic Synchronisation in a Rotor System with a Gear Coupling

E. Brommundt

Dedicated to the memory of Professor Friedrich Rimrott

Gear couplings transmit torque from driving to driven shafts whilst accommodating unavoidable misalignments and axial displacements. The friction forces at the sliding teeth transfer energy from the driving engine to the lateral oscillations of the shaft. Instability of the stationary motion, self-excitation, can result. The self-excited oscillations, in character related to the eigen-oscillations of the linear system, interact with the external excitation by unbalance forces. For a two degrees of freedom rotor-bearing system we show how to study systematically cases of higher-order synchronisation (frequency locking) which can help to interpret observed motions; numerical calculations and perturbation techniques are combined.

1 Introduction

Gear couplings consist of an externally toothed hub, see Fig.1a, and a mating sleeve with internal teeth which permit relative axial sliding. Crowning (rounding) of the hub teeth and a clearance (backlash) between the meshing gears prevent jamming and allow small angular displacements (*angular misalignments*) between the axes of sleeve and hub (see the angle α in Fig.1b; $|\alpha| < 0.004$ rad $\approx 0.25°$ at high speeds). The incorporation of the gear coupling into a rotor-bearing system has unwelcome side effects: The touching teeth-flanks need some slipping for lubrication, thus a minimum misalignment $|\alpha| > 0$ is necessary. The Coulomb type friction forces between the sliding tooth flanks introduce strictly non-linear effects into the otherwise linear rotor system. Like a shaft with internal friction (Ku et al., 1993) – rotating with an angular speed Ω – a rotor with a gear coupling will start to oscillate at a frequency ω_r as soon as Ω exceeds ω_r. As a rule, the relevant frequency ω_r is close to the natural frequency of that (linear) modal oscillation which draws most effectively energy from the power supply. Both, linear and non-linear terms of the equations of motion control the energy flow into the relevant mode and determine the amplitudes of the self-oscillation (of course, this depends on several system parameters). The frequency ω_r remains about fixed when Ω increases further, the self-oscillation appears as a *sub-harmonic oscillation*. (*Sub-harmonic* in contrast to the harmonic oscillations – at the frequency Ω – forced by the unbalances of the rotor.) In this paper we study the interaction of these two types of oscillation in a simple rotor system.

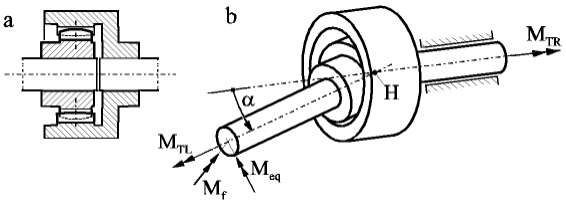

Fig. 1: Gear coupling; a) straight, b) displaced by angle α with moments applying to the left half, $M_{TL} \approx M_{TR} = M_T$

The bulk of literature on rotor systems with gear couplings concentrates on coupling alignment, lubrication and wear; e.g. Piotrowski (1995). Most of these publications contain no details about the vibrations which certainly accompany wear. A few authors report about instability and self-excited oscillations observed in plants; e.g. Shiraki et al. (1970). Common to all cases are the rather sudden onset of vibrations when the rotational speed of the rotor is increased, and the sub-synchronous frequency of the observed (self-excited) oscillations, independent of the speed Ω. Not all authors seem to identify the gear coupling as source of their trouble. Little literature exists on systematic investigations of self-excitation by gear couplings. Morton (1982) demonstrates by a four degrees of freedom rotor that a sufficiently large angular displacement of the coupling stabilizes the system; Yamauchi et al. (1981) study the dynamic characteristics of gear couplings analytically and experimentally.

The model of this paper is taken from Brommundt et al. (in preparation), where additional literature is listed. We use that model here to show how intricate oscillations, somewhat hidden in parameter space, can be uncovered by numerical means supported by perturbation techniques.

2 The Basics of Our System

2.1 The System

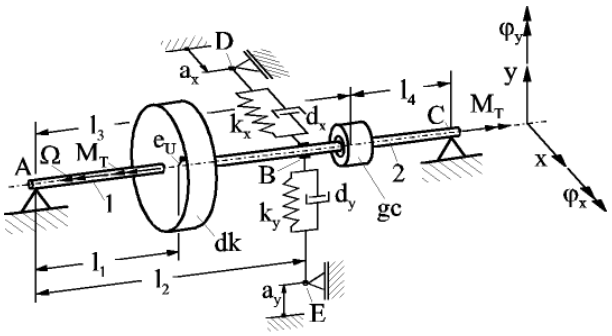

Fig.2: The system

The rotor shown in Fig.2 consists of two massless rigid shafts, No.1 and No.2, mounted on two rigid bearings A and C, and on the flexible bearing B, which is suspended by spring-dashpot elements. The attachment points D, E of the suspension elements can be slid by (a_x, a_y) to produce special (angular) misalignments in the gear coupling gc that connects the two shafts. Shaft 1 carries the rigid disk dk of a turbine, eccentricity e_U. The turbine drives the rotor with the constant speed (the angular velocity) Ω by a torque M_T which is consumed at the right hand side of the bearing C. Let Φ, the angle of rotation, be given by $\Phi = \Phi(t) = \Omega t$. A detailed set of parameters is listed in Appendix 1. (All numerical results base on these "nominal parameters", alterations only will be mentioned.)

2.2 Equations of Motion

The rotor deflections are measured by its displacements $x = x(t), y = y(t)$ at the bearing B with respect to the straight reference position $(x, y) = (0, 0)$, cf. Fig.2. The coupled non-linear second order differential equations

$$\begin{aligned} m\ddot{x} + d_x\dot{x} + \Omega\, J_p/l_2^2 \cdot \dot{y} + k_x(x - a_x) + M_F/l_2 \frac{\dot{x} + \Omega y}{v} \tanh(v/v^*) &= e_u m_u \Omega^2 \cos\Omega t, \\ m\ddot{y} + d_y\dot{y} - \Omega\, J_p/l_2^2 \cdot \dot{x} + k_y(y - a_y) + M_F/l_2 \frac{\dot{y} - \Omega x}{v} \tanh(v/v^*) &= e_u m_u \Omega^2 \sin\Omega t - W, \end{aligned} \tag{1}$$

$v := \sqrt{(\dot{x} + \Omega y)^2 + (\dot{y} - \Omega x)^2}$, govern the motions. They are taken from Brommundt et. al., see also Krämer (1993). The terms $\tanh(v/v^*)$ regularize (smoothen) the jump of the Coulomb friction at v = 0.

We introduce the configuration vector $\mathbf{u} = \mathbf{u}(t) = (x, y)^T$ and the state vector $\mathbf{v} = \mathbf{v}(t) = (\dot{\mathbf{u}}^T, \mathbf{u}^T)^T = (\dot{x}, \dot{y}, x, y)$. They are applied to abbreviate (1) in an obvious way by the following second, or first order differential equation, respectively:

$$\mathbf{M}\ddot{\mathbf{u}} + \mathbf{F}(\mathbf{u}, \dot{\mathbf{u}}, \Omega) + e_U \Omega^2 \mathbf{G}(\Omega t) = \mathbf{0}, \quad \dot{\mathbf{v}} = \mathbf{f}(\mathbf{v}) + e_U \Omega^2 \mathbf{g}(\Omega t). \tag{2), (3}$$

To compare magnitudes, it is advisable to work with non-dimensional quantities. We select as Reference quantities from the equations of motion the *mass* m, the (weight) *force* W, and the average *stiffness* $(k_x + k_y)/2$, respectively, and obtain the values (cf. the parameters in Appendix 1):

$$m_R = m = 50.19\,\text{kg}, F_R = W = 652.4\,\text{N}, k_R = (k_x + k_y)/2 = 25.25 \cdot 10^6\,\text{N/m}. \tag{4}$$

Auxiliary reference values are deduced: the angular frequency $\omega_R = \sqrt{k_R/m_R} = 709.3 \cdot \text{rad/s}$, the period $T_R = 2\pi/\omega_R = 8.86 \cdot 10^{-3}\,\text{s}$, the displacement $e_R = F_R/k_R = 25.8 \cdot 10^{-6}\,\text{m}$, and the velocity $v_R = e_R\omega_R = 18.32 \cdot 10^{-3}\,\text{m/s}$. Sometimes, we mark non-dimensional quantities by a tilde, e.g. $\tilde{t} = \omega_R \cdot t$.

2.3 Solutions for the Linear System

To become acquainted with our system we ask for its "linear behaviour" without the influence of the gear coupling effects, i.e. for $M_F = 0$ in (1): The *free vibrations*

$$\mathbf{u} = \breve{\mathbf{u}} \exp(\lambda t) \tag{5}$$

are two (couples of complex conjugate) eigen-solutions $(\lambda, \breve{\mathbf{u}})_k$, $\lambda_k = \sigma_k + j\omega_k$, k = 1, 2, (j := √ (-1)). Because of the gyroscopic effect they depend on the speed Ω. Here are values for $\tilde{\Omega} = \Omega/\omega_R = 0.0, 1.0, 2.0, 3.0$:

$$\begin{aligned}
\Omega/\omega_R = 0.0:\ \lambda_1/\omega_R &= -0.039 + 0.895j,\ \breve{\mathbf{u}}_1^T/e_R = (1,\ 0),\\
\lambda_2/\omega_R &= -0.064 + 1.093j,\ \breve{\mathbf{u}}_2^T/e_R = (0,\ 1);\\
\Omega/\omega_R = 1.0:\ \lambda_1/\omega_R &= -0.040 + 0.885j,\ \breve{\mathbf{u}}_1^T/e_R = (1,\ 0.013 + 0.208j),\\
\lambda_2/\omega_R &= -0.064 + 1.105j,\ \breve{\mathbf{u}}_2^T/e_R = (0.018 + 0.254j,\ 1);\\
\Omega/\omega_R = 2.0:\ \lambda_1/\omega_R &= -0.040 + 0.860j,\ \breve{\mathbf{u}}_1^T/e_R = (1,\ 0.017 + 0.366j),\\
\lambda_2/\omega_R &= -0.064 + 1.137j,\ \breve{\mathbf{u}}_2^T/e_R = (0.026 + 0.447j,\ 1);\\
\Omega/\omega_R = 3.0:\ \lambda_1/\omega_R &= -0.039 + 0.828j,\ \breve{\mathbf{u}}_1^T/e_R = (1,\ 0.017 + 0.474j),\\
\lambda_2/\omega_R &= -0.065 + 1.181j,\ \breve{\mathbf{u}}_2^T/e_R = (0.027 + 0.579j,\ 1).
\end{aligned} \tag{6}$$

Fig.3 shows the trajectories (x(t), y(t)) of the free vibrations for $\Omega/\omega_R = 1.0, 2.0, 3.0,$ starting at the point ○. For λ_1 circulate the trajectories clockwise, i.e. opposite to the rotation of the shaft, for λ_2 coincide both directions. The *forced harmonic oscillations,* due to the unbalance, have the form

$$\begin{aligned}
x_U &= \hat{x}_c \cos(\Omega t) + \hat{x}_s \sin(\Omega t) = \hat{x} \cos(\Omega t + \alpha_x),\\
y_U &= \hat{y}_c \cos(\Omega t) + \hat{y}_s \sin(\Omega t) = \hat{y} \cos(\Omega t + \alpha_y),
\end{aligned} \tag{7}$$

see Fig.4.

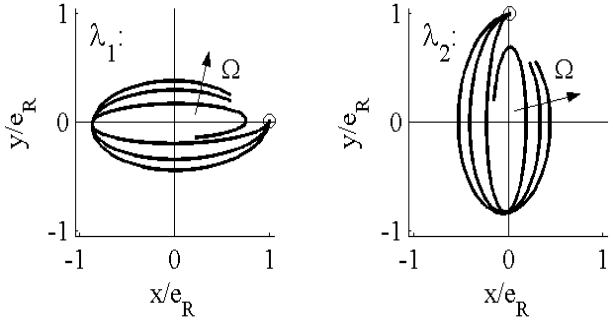

Fig.3: Free vibrations of the linear system

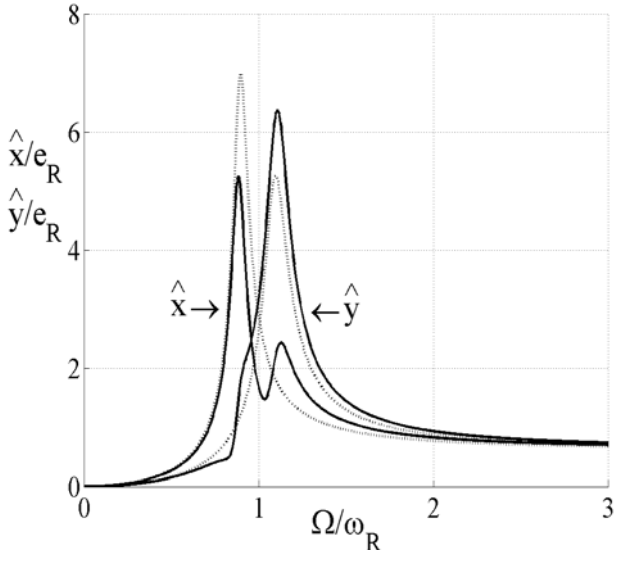

Fig.4: Amplitudes $\hat{x}(\Omega), \hat{y}(\Omega)$ of the forced oscillations

3 The Behaviour of the Perfectly Balanced System

Perfect balance means $e_U = 0$ in (1). Furthermore, we assume $a_x = 0$ and sum the effects of the weight W and the adjustment a_y. Their combined action is captured by the parameter m_a (it steers the misalignment):

$$m_a W = W - a_y k_y . \tag{8}$$

Then, equation (1) gets the form

$$\begin{aligned} m\ddot{x} + d_x\dot{x} + \Omega J_p/l_2^2 \cdot \dot{y} + k_x x + M_F/l_2 \frac{\dot{x} + \Omega y}{v} \tanh\left(v/v^*\right) &= 0, \\ m\ddot{y} + d_y\dot{y} - \Omega\ J_p/l_2^2 \cdot \dot{x} + k_y y + M_F/l_2 \frac{\dot{y} - \Omega x}{v} \tanh\left(v/v^*\right) &= -m_a W. \end{aligned} \tag{9}$$

3.1 The Stationary Solution and its Stability

The autonomous equation (9) has the stationary solution

$$\mathbf{u}_0 = (x_0, y_0)^T = (\rho\cos\gamma, -\rho\sin\gamma), \tag{10}$$

where ρ and γ follow from

$$\begin{aligned} \left(k_x k_y \rho^2 + \left((M_F/l_2)\tanh(\Omega\rho/v^*)\right)^2\right) \Big/ \sqrt{k_x^2\rho^2 + \left((M_F/l_2)\tanh(\Omega\rho/v^*)\right)^2} &= m_a W, \\ \tan\gamma = k_x\rho \Big/ \left((M_F/l_2)\tanh(\Omega\rho/v^*)\right). \end{aligned} \tag{11}$$

To investigate the stability of $\mathbf{u}_0$ it is disturbed by $\delta\mathbf{u}$, and the behaviour of perturbed solution $\mathbf{u} = \mathbf{u}_0 + \delta\mathbf{u}$ is obtained from the variational equation, cf. (1) and (2),

$$\mathbf{M}\,\delta\ddot{\mathbf{u}} + \mathbf{F}_{\dot{\mathbf{u}}}(\mathbf{u}_0, \mathbf{0}, \Omega)\,\delta\dot{\mathbf{u}} + \mathbf{F}_{\mathbf{u}}(\mathbf{u}_0, \mathbf{0}, \Omega)\,\delta\mathbf{u} = \mathbf{0}, \tag{12}$$

where $\mathbf{F}_{\dot{\mathbf{u}}}$ and $\mathbf{F}_{\mathbf{u}}$ are Jacobi matrices of $\mathbf{F}$ with respect to $\dot{\mathbf{u}}$ and $\mathbf{u}$ at the constant displacement $\mathbf{u}_0$ (the details are a bit lengthy). The displacement $\mathbf{u}_0$ is stable (with respect to sufficiently small perturbations) when all eigen-solutions $\delta\mathbf{u} = \hat{\mathbf{u}}\exp(\lambda t)$ decay, i.e., when $\sigma_k := \mathrm{Re}\,\lambda_k < 0,\ \text{for } k = 1,\ldots,4.$

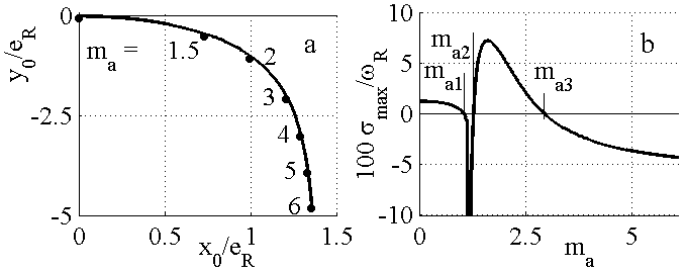

Fig.5: Stationary solution; a) displacement, b) real-part σ_{max}

As an example, Fig.5 demonstrates some results calculated for $\Omega = 0.5\cdot\Omega_N; \Omega_N$ – nominal speed. Fig.5a shows the stationary displacement (x0, y0) of the bearing B as it changes when m_a is increased from 0 to 6: the suspension point E of the (initially weightless) rotor is shifted from zero to a value equivalent to a rotor displacement caused by a 6-fold weight. (The bullet at (x0, y0) ≈ (0, 0) holds for $m_a = 1$ where the coupling nearly sticks.) Fig.5b shows σ_{max}, the largest real-part of the eigen-values, as function of m_a. Except for the small gap between $m_{a1} = 1.05$ and $m_{a2} = 1.28$, σ_{max} is positive up to $m_{a3} = 2.93$. Throughout the region $0 < m_a < m_{a3}$ the stationary displacement is unstable. (A careful study of the stable stationary solution within the gap between m_{a1} and m_{a2} reveals that it has a very small domain of attraction only: any not so small disturbance upsets $\mathbf{u}_0$.)

Remark 1: Here, a value $m_a > 3$ stabilises the stationary displacement. An $m_a = 3$ leads to an angle α of less than 0.1° (cf. the Introduction). Thus, an appropriately chosen m_a seems to be a remedy against instability, generally applicable. But the magnitude of m_a is limited by the heat generation in the coupling (cf. Czerny, 1993)!

3.2 Self-Excited Oscillations

For $\Omega = 0.5 \cdot \Omega_N$ and $m_a = 1$, a point in the unstable region of Fig.5b, we solve the non-linear differential equation (9) numerically. The initial state $\mathbf{v}^0 = \mathbf{v}(0)$ is chosen such that it differs little from the stationary state of Fig.5a – corresponding to a small perturbation – but leads to clear diagrams. Fig.6 presents the motions for the first 40 revolutions of the transition from the phase point near the stationary state to the (periodic) limit cycle shown in Fig.6d:

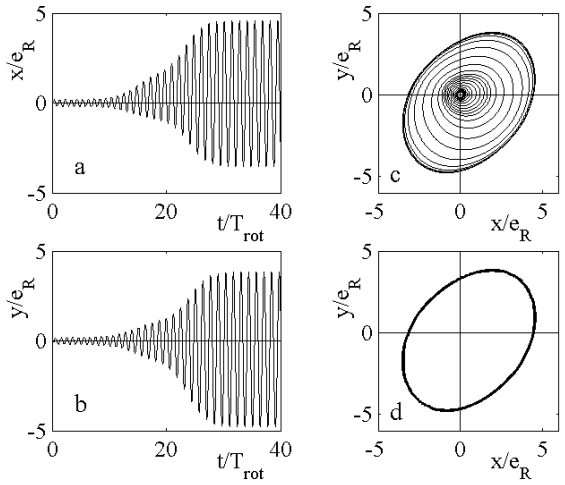

Fig.6: Self-excited oscillations: a) $x(t)$ horizontal, b) $y(t)$ vertical, c) the trajectory $(x(t), y(t))$, d) the clockwise rotating limit cycle, cf. (13)

$$\begin{aligned} &\big(x(t), y(t)\big) = \big(x(t+T_S), y(t+T_S)\big), \\ &T_S = 5.70\,T_R,\ \omega_S = 2\pi/T_S = 1.10\,\omega_R, \\ &T_{rot} = 4.36\,T_R,\ \Omega = 2\pi/T_{rot} = 1.49\,\omega_R. \end{aligned} \tag{13}$$

T_S, ω_S – period, frequency of the self-excited oscillation, T_{rot}, Ω – period, frequency of the rotation.

The frequency ω_S, $\omega_S = 1.10\,\omega_R$, is close to the frequency $\omega_2 \approx 1.12\,\omega_R$ of the second normal mode, cf. (6). The elliptical limit cycle circulates in the same direction and has a similar convexity as the corresponding modal oscillation , cf. λ_2 in Fig.3; it is just tilted against the direction of the rotation. The amplitudes of the self-oscillation have about the same magnitude as the resonant peaks in Fig.4.

Below, in Sect.4.3, we shall abbreviate the periodic limit cycle (of the self-excited oscillation) by

$$\mathbf{p} = \mathbf{p}(t) = \big(x_p(t), y_p(t)\big)^T. \tag{14}$$

4 The Behaviour of the Unbalanced System

4.1 Some Numerical Explorations

What will the rotor motion look like when the self-oscillation and the periodic excitation by the unbalance interact ? To calculate distinct – and not so simple – results, we choose the parameters $m_a = 1$, cf. (8), $\Omega = 0.73 \cdot \Omega_N$, i.e. $T_{rot} = 2.99\ T_R$, and $e_U = 2 \cdot e_{UN}$. The latter both are selected such that we are not too far above the (linear) resonance, see Fig.4, but retain the unbalance force which varies with Ω^2.

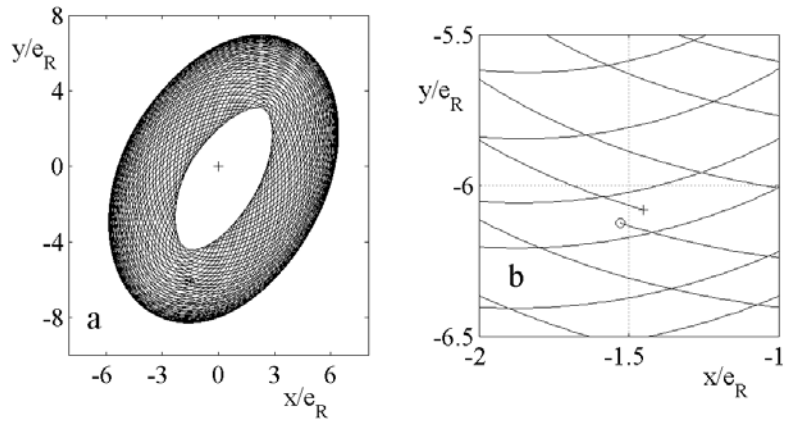

Fig.7: Stationary oscillations; a) trajectory $(x(t), y(t))$, b) enlarged: trajectory near $\mathbf{u}(0)$, marked o, and $\mathbf{u}(T_1)$, $T_1 = 109 \cdot T_{rot}$, marked +

To get rid of transient effects and arrive at a stationary motion, we solve the initial value problem for equation (1) with $\mathbf{v}(0) = \mathbf{0}$ for the time interval $0 \le t \le t_E$, with $t_E = 150 \cdot T_{rot}$, which leads to a suitable starting state $\mathbf{v}^0 = \mathbf{v}(t_E) \Rightarrow \mathbf{v}(0)$ for $(t - t_E) \Rightarrow t$, i.e. the new (shifted) time axis.

Fig.7a shows the trajectory $\mathbf{u} = \mathbf{u}(t) = (x(t), y(t))^T$ for $0 \le t \le T_1$, where $T_1 = 109 \cdot T_{rot}$, i.e. for 109 rotor revolutions. The structure of the trajectory $\mathbf{u}(t)$ is understood best when $\mathbf{u}(t)$ is conceived as a curve in 3D space

where it winds, torus-like, around the limit cycle of Fig.6d, and Fig.7a is just a projection of the space curve to the x-y-plane (cf. Ioos et al., 1980). On the torus the *longitude* measures the progress in the direction of the limit cycle, the *latitude* measures the winding. During the 109 rotor revolutions the trajectory cycles the torus (in the longitudinal direction) 58 times.

Fig.7b presents an enlarged neighbourhood of the initial point "o" and the endpoint "+" of the trajectory: The trajectory misses periodicity by a narrow margin. But, the (nearly) parallel sections of $\mathbf{u}(t)$ look very regularly spaced, their lateral distances satisfy about the ratio 3:8:11. Thus, the trajectory should close after a 10-fold repetition, i.e. after 1090 revolutions.

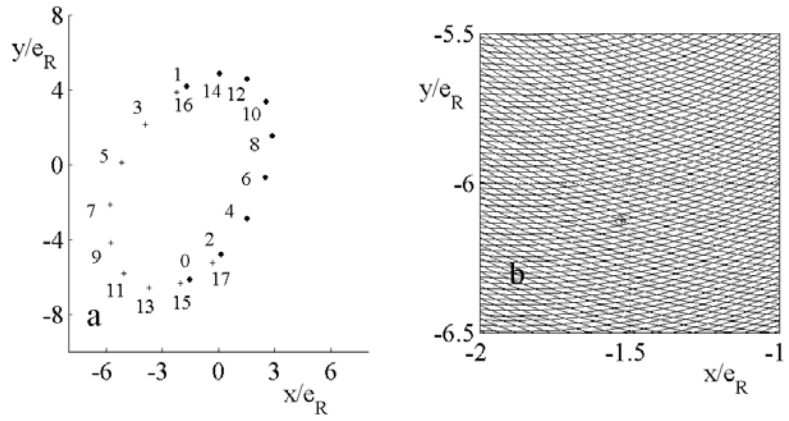

Fig.8: Some details of the completed orbit of Fig.7, same scale;
a) Configurations $\mathbf{u}(k \cdot T_{rot})$ for k = 0 to 17, points □ (even), + (odd),
b) Period points o, at $\mathbf{u}(0)$, and +, at $\mathbf{u}(1058 \cdot T_{rot})$, coincide accurately

The corresponding calculation reveals that the trajectory closes already after n_{SH} = 1058 revolutions. Fig.8b shows that the initial point "o" and the endpoint "+" of the orbit agree very accurately. During that period the trajectory cycles the torus m_{SH} = 563 times. (The orbit can not be shown in print since its torus is all blacked by lines; cf. Fig.7a.)

Fig.8a – drawn at the same scale as Fig.7a – shows how the period-points $\mathbf{u}(k \cdot T_{rot})$, k = 0 to 17, wander along an oval curve. This wandering is responsible for the deviation of the number $n_{SH} = 1058$ from the estimation 1090 above.

The found solution $\mathbf{u}(t)$ has the period

$$T_{SH} = n_{SH} T_{rot}: \quad \mathbf{u}(t) = \mathbf{u}(t + T_{SH}); \tag{15}$$

we denote it by $\mathbf{q}(t; m_{SH}, n_{SH})$. Because of

$$\omega_{SH} = 2\pi / T_{SH} = 2\pi / (n_{SH} T_{rot}) = \Omega / n_{SH}\ , \tag{16}$$

$$\mathbf{q}(t; m_{SH}, n_{SH}) = \mathbf{q}(t + T_{SH}; m_{SH}, n_{SH}) = \mathbf{q}(t + 2\pi/\omega_{SH}; m_{SH}, n_{SH}) \tag{17}$$

is *sub-harmonic of the order* n_{SH} with respect to the excitation in (1), which runs with the speed Ω, the angular frequency of the rotation. The frequency ω_S of the original self-excited oscillation, cf. (13), (14), hides behind the above m_{SH} cycles:

$$\omega_S = m_{SH}\, \omega_{SH} \ = m_{SH} / n_{SH} \cdot \Omega, \text{ and } T_S = T_{SH} / m_{SH} = n_{SH} / m_{SH} \cdot T_{rot}. \tag{18}$$

The numbers from above lead to $\omega_S = 1.12\ \omega_R$, cf. ω_2 in (6), but now it is – or has become – a rational multiple of the exciting frequency Ω. What will happen when Ω is changed slightly ?

4.2 Tracing of Sub-Harmonic Oscillations at Parameter Variations

We want to trace a discrete sub-harmonic oscillation along parameter variations, especially along changes of the exciting frequency Ω. The example of Sect. 4.1 is far too lengthy for this purpose. Therefore, we begin with the sub-harmonic oscillation $\mathbf{q}(t; 4, 5)$, cf. Fig.9, calculated for $\Omega = 0.47 \cdot \Omega_N$, $T_{rot} = 4.64\ T_R$.

The states $\mathbf{v}_{(4,5)}(t)$ to the sub-harmonic solutions $\mathbf{q}(t; 4, 5)$ satisfy the periodicity condition (16), (17):

$$\mathbf{v}_{(4,5)}(0) = \mathbf{v}_{(4,5)}(2\pi\, n_{SH} / \Omega). \tag{19}$$

Solutions to the differential equation (1), for $\Omega + \Delta\Omega$, which satisfy the periodicity condition (19) are obtained via the shooting method (Deuflhard et al. 2002) by Newton iterations (Deuflhard et al. 2003): the initial values $\mathbf{v}_{(4,5)}(0)$ thus calculated for Ω serve as starting point for $\Omega + \Delta\Omega$; tiny steps $\Delta\Omega$ only are allowed. The variational equation

$$\mathbf{M}\,\delta\ddot{\mathbf{u}} + \mathbf{F}_{\mathbf{u}}(\mathbf{q},\dot{\mathbf{q}},\Omega)\,\delta\dot{\mathbf{u}} + \mathbf{F}_{\mathbf{u}}(\mathbf{q},\dot{\mathbf{q}},\Omega)\,\delta\mathbf{u} = \mathbf{0} \tag{20}$$

has to be solved parallel to (1) to yield the Newton matrix for the shooting procedure, as well as for the calculation of the characteristic multipliers $\mu_k(\Omega)$ for the stability investigation, cf. Farkas (1994). These continuations of $\mathbf{q}(t; 4, 5)$ converge only over the very narrow interval

$$L_{(4,5)} = \{\, \Omega: 0.4698 < \Omega < 0.471... \}. \tag{21}$$

The interval $L_{(m,n)}$ is the *locking region* where the frequency ω_{SH} of the sub-harmonic is *locked* to the excitation Ω as given by (16), cf. Sect. X.15 in Ioos et al. (1980). [Compared to Fig.9, the shape of the solution changes appreciably along $L_{(4,5)}$.] At the borders of the interval the solution $\mathbf{q}(t; 4, 5)$ becomes unstable, $\mu_{max}(\Omega)$, the

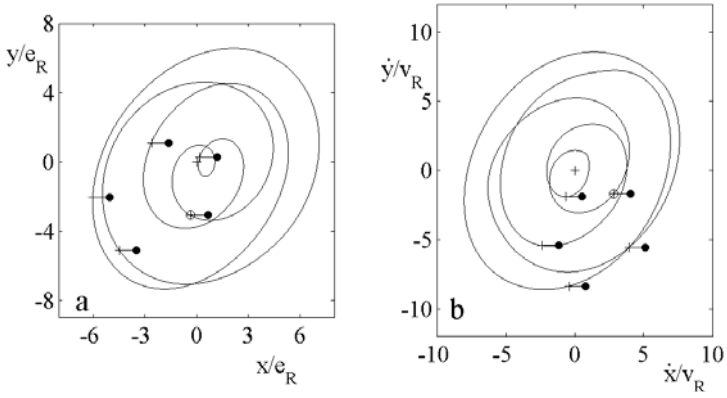

Fig.9: Sub-harmonic $\mathbf{q}(t; 4, 5)$: a) orbit, b) hodograph; + • show 5 positions of the eccentricity

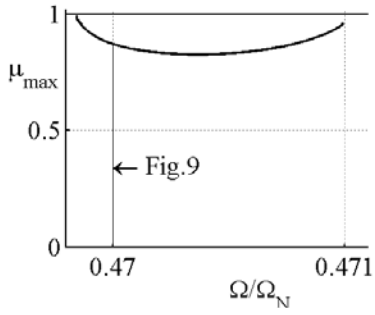

Fig.10: Characteristic multiplier

largest characteristic multiplier, gets > 1, cf. Fig.10. For the immediate neighbourhoods of $L_{(4,5)}$ the shape of $\mathbf{q}(t; 4, 5)$ converts (numerically!) to high-order sub-harmonics like the one shown in Sect. 4.1. Their locking regions, although very narrow too, seem even to overlap with $L_{(4,5)}$. Quasi-periodic solutions with unlocked frequencies Ω and ω_S could not be detected; cf. Fig.X.3 in Ioos et al. (1980).

Remark 2: The computation of Ω_0 by (29), cf. Fig.11b, yields $\Omega_0 = 0.4656 \cdot \Omega_N$, which lies well outside $L_{(4,5)}$.

4.3 A Systematic Search for Sub-Harmonic Oscillations

Since the locking regions are very narrow, it is difficult to calculate on purpose, for given (m_{SH}, n_{SH}), the sub-harmonic $\mathbf{q}(t; m_{SH}, n_{SH})$; see Remark 2. We outline a procedure to find such oscillations systematically. It combines perturbation techniques (related to Ch.6 of Farkas 1994) with numerical calculations. We proceed in 3 steps: i) A small parameter ε is introduced into the equation of motion which permits to treat the forced oscillation as a perturbation of the limit cycle. ii) We choose the Example $(m_{SH}, n_{SH}) = (13, 16)$, close to the above $(m_{SH}, n_{SH}) = (4, 5)$; compare: (13/16):(4/5) = 65/64. For the Example we evaluate the formal expressions of the perturbation terms numerically. iii) The numerically obtained terms are applied to compute, for $\varepsilon = 0.1$, a solution $\mathbf{q}(t, \varepsilon; 13, 16)$ which is continued to larger ε by gradual increase, $\varepsilon = 0.1, ..0.2, ..0.3, ..$, and iteration with the complete equation of motion (equation (22) below).

Remark 3: In this Section 4.3, the calculation of periodic solutions by Fourier expansions is beneficial (cf. Urabe, 1963); see Appendix 2.

First, in equation (2) we multiply the excitation by the small parameter ε and decompose the forcing term:

$$\mathbf{M}\,\ddot{\mathbf{u}} + \mathbf{F}(\mathbf{u},\dot{\mathbf{u}},\Omega) + \varepsilon\, e_U m_U \Omega^2 \left(\mathbf{r}_c \cos(\Omega t + \alpha) + \mathbf{r}_s \sin(\Omega t + \alpha)\right) = \mathbf{0};\ \ \mathbf{r}_c := (1,0)^T, \mathbf{r}_s := (0,1)^T; \tag{22}$$

$\varepsilon = 0$ leads to the autonomous system of Sect.3, $\varepsilon = 1$ leads to the original unbalanced (the forced) system. (The phase angle α will be needed later.) Next, we introduce the non-dimensional time τ such that the period T_{SH} of $\mathbf{q}(t,\varepsilon;m_{SH},n_{SH})$ is transformed to 2π:

$$\tau = \Omega t / n_{SH},\ \ \mathbf{q}(\tau,\varepsilon;m_{SH},n_{SH}) = \mathbf{q}(\tau + 2\pi,\varepsilon;m_{SH},n_{SH}),\ \ (.)' := d(.)/d\tau. \tag{23}$$

Equation (22), for $\mathbf{u}(\tau,\varepsilon)$, reads now

$$\Omega^2 / n_{SH}^2 \cdot \mathbf{M}\,\mathbf{u}'' + \mathbf{F}\left(\mathbf{u}, \Omega / n_{SH} \cdot \mathbf{u}', \Omega\right) + \varepsilon\, e_U m_U \Omega^2 \left(\mathbf{r}_c \cos(n_{SH}\tau + \alpha) + \mathbf{r}_s \sin(n_{SH}\tau + \alpha)\right) = \mathbf{0}. \tag{24}$$

We assume $\Omega = \Omega(\varepsilon)$ and expand $\mathbf{u}(\tau,\varepsilon), \Omega(\varepsilon)$ with respect to ε up to the first order:

$$\mathbf{u}(\tau,\varepsilon) = \mathbf{u_0}(\tau) + \varepsilon\, \mathbf{u}_1(\tau) + \ldots,\ \ \Omega(\varepsilon) = \Omega_0(1 + \nu_1\varepsilon + \ldots). \tag{25}$$

Then follow from (24)

$$\varepsilon^0:\ \ \Omega_0^2 / n_{SH}^2 \cdot \mathbf{M}\,\mathbf{u}_0'' + \mathbf{F}\left(\mathbf{u}_0, \Omega_0 / n_{SH} \cdot \mathbf{u}_0', \Omega_0\right) = \mathbf{0}, \tag{26}$$

$$\begin{aligned} \varepsilon^1:\ & \Omega_0^2 / n_{SH}^2 \cdot \mathbf{M}\,\mathbf{u}_1'' + \mathbf{F}_{\mathbf{u}'}\left(\mathbf{u}_0, \Omega_0 / n_{SH} \cdot \mathbf{u}_0', \Omega_0\right) \cdot \Omega_0 / n_{SH} \cdot \mathbf{u}_1' + \mathbf{F}_{\mathbf{u}}\left(\mathbf{u}_0, \Omega_0 / n_{SH} \cdot \mathbf{u}_0', \Omega_0\right) \cdot \mathbf{u}_1' = \\ & = -\nu_1 \left(2 \cdot \Omega_0^2 / n_{SH}^2 \cdot \mathbf{M}\,\mathbf{u}_0'' + \mathbf{F}_{\mathbf{u}'}\left(\mathbf{u}_0, \Omega_0 / n_{SH} \cdot \mathbf{u}_0', \Omega_0\right) \cdot \Omega_0 / n_{SH} \cdot \mathbf{u}_0' + \mathbf{F}_{\Omega}\left(\mathbf{u}_0, \Omega_0 / n_{SH} \cdot \mathbf{u}_0', \Omega_0\right) \cdot \Omega_0\right) \\ & \quad + e_U m_U \Omega_0^2 \left(\mathbf{r}_c \cos(n_{SH}\tau + \alpha) + \mathbf{r}_s \sin(n_{SH}\tau + \alpha)\right). \end{aligned} \tag{27}$$

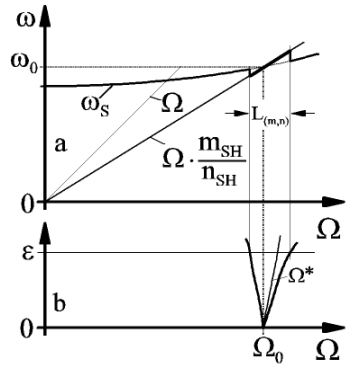

Fig.11: Frequency dependences, a) self-excitation $\omega_S(\Omega)$; b) wedge-like region of entrainment

Equation (26) is equal to equation (9), the self-excited autonomous system of Sect.3, in the disguise of (2) and (23). After the transformation $(23)_1$, the periodic solution $\mathbf{u}_0(t) = \mathbf{p}(t)$, the limit cycle (14), satisfies

$$\mathbf{p}(t) = \mathbf{p}(t + 2\pi/\omega_S),\ \mathbf{p}(t) = \mathbf{p}(\tau \cdot n_{SH}/\Omega) \Rightarrow \mathbf{p}(\tau)\ \text{below}. \tag{28}$$

The frequency ω_S depends on the speed Ω: $\omega_S = \omega_S(\Omega)$, cf. Fig.11a. Now, ω_S must meet $(18)_1$, depicted in Fig.11a by the straight line $\omega = \Omega \cdot m_{SH}/n_{SH}$ through the origin. To compute the intersection (Ω_0, ω_0) from $\omega_S(\Omega) = \Omega \cdot m_{SH}/n_{SH}$ we fix the phase of $\mathbf{p}(t)$ by the condition $\dot{y}_p(0) = c_0, c_0 - \text{constant}$ and solve the set of 5 equations

$$\mathbf{v}_p(0) = \mathbf{v}_p(2\pi/\omega_S),\ \ \omega_S(\Omega) = \Omega \cdot m_{SH}/n_{SH}, \tag{29}$$

for $\left(\dot{x}_p(0), x_p(0), y_p(0), \omega_S, \Omega\right)$ by an appropriately modified shooting method. From the computations result the frequencies $(\omega_0, \Omega_0) = (1.072\,\omega_R, 0.458\,\Omega_N)$, cf. Fig.11a, and the pertinent limit cycle $\mathbf{p}(\tau) = \mathbf{p}(\tau + 2\pi/m_{SH})$ recorded by means of its Fourier coefficients (cf. Appendix 2 for the notations),

$$\mathbf{f}_{cp} = \mathbf{A}^{\mathbf{F}}\,\mathbf{p}(\tau). \tag{30}$$

Next, we have to solve equation (27): Its left side, the homogeneous linear periodic variational equation

$$\Omega_0^2/n_{SH}^2 \cdot \mathbf{M}\,\mathbf{u}_1'' + \mathbf{F}_{\mathbf{u}'}\left(\mathbf{p}(\tau), \Omega_0/n_{SH}\cdot\mathbf{p}'(\tau), \Omega_0\right)\cdot\Omega_0/n_{SH}\cdot\mathbf{u}_1' + \mathbf{F}_{\mathbf{u}}\left(\mathbf{p}(\tau), \Omega_0/n_{SH}\cdot\mathbf{p}'(\tau), \Omega_0\right)\cdot\mathbf{u}_1' = \mathbf{0}, \quad (31)$$

has the four Floquet solutions (cf. Jordan et al. (1987); here are all numerical results expressed by state vectors):

$$\mathbf{v}_{F,k}(\tau) = \mathbf{\Phi}_\mathbf{k}(\tau)\cdot\exp(\lambda_k\tau),\ \mathbf{v}_{F,k}(2\pi) = \mu_k\mathbf{v}_{F,k}(0),\ \mu_k = \exp(\lambda_k 2\pi),\ k = 1,...,4, \quad (32)$$

λ_k – characteristic exponent, μ_k – characteristic multiplier, $\mathbf{\Phi}_\mathbf{k}(\tau) = \mathbf{\Phi}_\mathbf{k}(\tau + 2\pi)$; the first Floquet solution, $\mathbf{v}_{F,1}(\tau)$, is the derivative of $\mathbf{p}(\tau)$:

$$\mathbf{v}_{F,1}(\tau) = \left(\mathbf{p}''^{\mathbf{T}}(\tau), \mathbf{p}'^{\mathbf{T}}(\tau)\right)^T,\ \lambda_1 = 0,\ \mu_1 = 1. \quad (33)$$

The particular solution to the non-homogeneous equation (27) we split into the parts $\mathbf{v}_{\nu_1}(\tau)$ and $\mathbf{v}_{e_U}(\tau)$ holding for $(\nu_1, e_U) = (-1, 0)$ and $(\nu_1, e_U) = (0, e_U)$, respectively; both computed with the initial conditions $\mathbf{v}_{\nu_1}(0) = \mathbf{0}$, $\mathbf{v}_{e_U}(0) = \mathbf{0}$.

The general solution to equation (27) gets the form

$$\mathbf{v}_{\mathbf{u}_1}(\tau) = \sum_{k=1}^{4} c_k\mathbf{v}_{F,k}(\tau) - \nu_1\mathbf{v}_{\nu_1}(\tau) + \mathbf{v}_{e_U}(\tau). \quad (34)$$

To become part of the sub-harmonic solution, cf. $(25)_1$, $\mathbf{u}_1(\tau)$, thus $\mathbf{v}_{\mathbf{u}_1}$, must be 2π-periodic:

$$\mathbf{v}_{\mathbf{u}_1}(2\pi) = \mathbf{v}_{\mathbf{u}_1}(0). \quad (35)$$

These are 4 conditions for the 5 free constants c_k and ν_1 of (34). Because of (33), for infinitesimally small c_1, the term $c_1\,\mathbf{v}_{F,1}(\tau)$ corresponds to an infinitesimally small phase shift of $\mathbf{p}(\tau)$, but (relative) phase shifts between $\mathbf{p}(\tau)$ and the forcing terms are taken into account already by the angle α in (22). Therefore, we choose $c_1 = 0$ and compute the other 4 constants from

$$\left(\mathbf{v}_{\nu_1}(2\pi), (1-\mu_2)\mathbf{\Phi}_2(0), (1-\mu_3)\mathbf{\Phi}_3(0), (1-\mu_4)\mathbf{\Phi}_4(0)\right)\left(\nu_1, c_2, c_3, c_4\right)^T = \mathbf{v}_{e_U}(2\pi). \quad (36)$$

With the known c_k follows from (34), (32) the initial vector $\mathbf{v}_{\mathbf{u}_1}(0) = \sum_{k=2}^{4} c_k\mathbf{\Phi}(0)$ which leads by numerical integration of (27) to

$$\mathbf{u}_{p1}(\tau) = \mathbf{u}_{p1}(\tau + 2\pi), \quad (37)$$

and its Fourier coefficients

$$\mathbf{f}_{cu_1} = \mathbf{A}^\mathbf{F}\mathbf{u}_{p1}(\tau). \quad (38)$$

Here are some results for $(m_{SH}, n_{SH}) = (13,16)$ and $\alpha = \pi/4$: The 4 multipliers μ_k are (1.00000002, $5.4\cdot10^{-5}$, $2.7\cdot10^{-10}$, $-5.7\cdot10^{-11}$). The first multiplier agrees very accurately with condition $(33)_3$: $\mu_1 = 1$. The remaining three multipliers are small because of the long period T_{SH} and the comparatively large damping. For ν_1 we obtain the small value $\nu_1 = 1.6\cdot10^{-7}$. [Additional calculations show $|\nu_1| < 2\cdot10^{-7}$ for the whole region $-\pi < \alpha \le \pi$; thus, the acute angle at the tip of the wedge in Fig.11b is very sharp.]

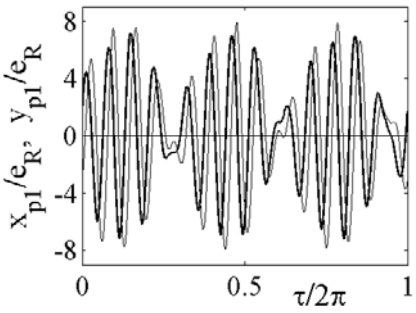

Fig.12: Function $\mathbf{u}_{p1}(\tau) = (x_{p1}(\tau), y_{p1}(\tau))^T$, x_{p1}: thick line, y_{p1}: thin line

Fig.12 shows the functions $\mathbf{u}_{p1}(\tau) = (x_{p1}(\tau), y_{p1}(\tau))^T$. The Fourier-terms of the 13th and the 16th order dominate in $\mathbf{u}_{p1}(\tau)$, they have about the same magnitude. That leads to the (16-13)th = 3rd order beat-like 'envelopes' which can be recognized along $x_{p1}(\tau)$ and $y_{p1}(\tau)$.

For step iii) we obtain by (28), (38) from $(25)_1$ $\mathbf{q}(\tau, \varepsilon; m_{SH}, n_{SH}) = \mathbf{p}(\tau) + \varepsilon \mathbf{u}_{p1}(\tau)$, after Fourier expansion:

$$\mathbf{f}_{cq} = \mathbf{f}_{cp} + \varepsilon \mathbf{f}_{cp1}. \tag{39}$$

In numerical form, this is a suitable starting vector for the iterative solution to equation (A.4):

$$\mathbf{f}_{cH}(\mathbf{f}_{cq}, \Omega, \varepsilon) = \mathbf{0}. \tag{40}$$

Remark 4: Initially, at small ε, the excitation is too weak to keep $\mathbf{q}(\tau, \varepsilon)$ in phase during the Newton steps, the iterations do not converge. Therefore, *one* of the large Fourier coefficients $a_{x,n_{SH}}, b_{x,n_{SH}}, a_{y,n_{SH}}$, or $b_{y,n_{SH}}$, that originate from the limit cycle, is kept fixed. Its place, as an unknown variable in (40), is taken by Ω, which varies now as function of ε: $\Omega = \Omega^*(\varepsilon)$.

Table 1 shows numerical values of the frequency $\Omega^*(\varepsilon)$ for $\varepsilon = (0 : 0.1 : 0.5)$. Although, by magnitude, the variation is small, the curve $\Omega^*(\varepsilon)$ in Fig.11b is obviously bent to the right. (The locking region $L_{(13,16)}$ is not calculated; cf. Remark 2.)

ε	0	0.1	0.2	0.3	0.4	0.5
Ω^*/Ω_N	0.4578	0.4578	0.4579	0.4582	0.4585	0.4591

Table 1: Frequency dependence $\Omega^*(\varepsilon)$ for $\mathbf{q}(\tau, \varepsilon; 13/16)$

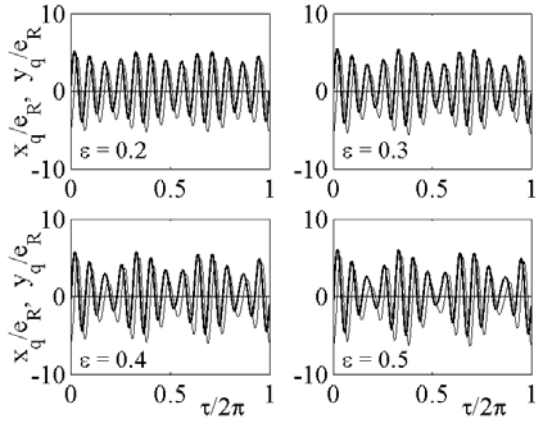

Fig.13: Sub-harmonic oscillations $\mathbf{q}(\tau, \varepsilon; 13/16)$; compare with Fig.12

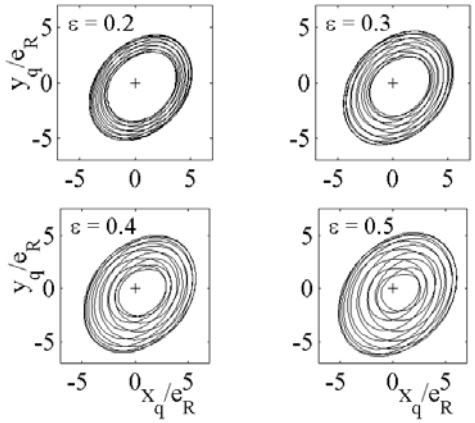

Fig.14: Sub-harmonic orbits $(x_q(\tau), y_q(\tau))$

Fig.13 demonstrates how the character of the sub-harmonic oscillation changes when $\varepsilon = (0.2 : 0.1 : 0.5)$ – the amplitude of the external excitation – grows: At $\varepsilon = 0.2$ is the limit cycle with its 13 cycles still dominant, at $\varepsilon = 0.5$ are the envelopes of Fig.12, the beats, clearly visible. The tori in Fig.14 do not change drastically when ε grows, they just get thicker, the lines spread apart.

5 Conclusions

In the unstable region of a rotor system with a gear coupling interact the self-excitation and the external excitation by unbalance forces. High-order sub-harmonic synchronizations with very narrow locking regions occur. Depending on the relative amplitudes of the limit cycle and the forced part of the oscillations, beat-like oscillations can happen. There are rapid variations of the character of the oscillations when the speed varies.

To study the above phenomena, a method is developed which permits to calculate sub-harmonic oscillations of given frequency ratios systematically. Perturbation techniques combine with numerical calculations. Urabe's Fourier-Galerkin expansions turn out as a favorable means to calculate and extrapolate periodic solutions of non-linear differential equations.

Appendix 1: Parameters and Reference values:

The following set of *nominal parameters* was suggested by Prof. Dr. E. Krämer, Darmstadt. (More details will be provided in Brommundt et. al.) For Fig.2 and equation (1) hold:

Longitudinal dimensions: $l_1 = 0.4$ m, $l_2 = 0.8$ m, $l_3 = 1.1$ m, $l_4 = 0.9$ m, $e_u = 16\cdot10^{-6}$ m;
Mass and Inertia: $m_{dk} = 100$ kg, $J_d = 1.60$ kg m^2, $J_p = 3.13$ kg m^2, $m_{gc} = 12$ kg, $g = 9.81$ m/s^2;
Bearing suspension: $k_x = 20.25\cdot10^6$ N/m, $k_y = 30.25\cdot10^6$ N/m, $d_x = 2.81\cdot10^3$ Ns/m, $d_y = 4.58\cdot10^3$ Ns/m;
Coupling: torque $M_T = 3920$ N m, friction $\mu_0 = 0.10$, diameter $d_{gc} = 0.18$ m, smoothing $v_{rel}^* = 0.01$ mm/s, pressure angle $\alpha_0 = 20°$;
Nominal speed $n = 19\,500$ rpm $\rightarrow$ $\Omega_N = 2042$ rad/s $= 2.8789\cdot\omega_R$, cf. (4);
adjustments $a_x = 0$, $a_y = 0$, or special choices.

Several parameters of the equations of motion are combinations of the above parameters:

$$\begin{aligned} &m = m_{dk}(l_1/l_2)^2 + m_{gc}(l_3/l_2)^2 + J_d/l_2^2;\ m_u = m_{dk}(l_1/l_2);\ W = g(l_1 m_{dk} + l_3 m_{gc})/l_2; \\ &M_F = 2/(\pi\cdot\cos\alpha_0)\cdot|M_T|\cdot\mu_0\cdot(1+l_3/l_4);\ v^* = 2\,v_{rel}\,l_2/d_{gc}\,l_4/(l_3 + l_4). \end{aligned} \tag{A.1}$$

Appendix 2: Notations for the Fourier Expansions; Galerkin Projection

We approximate 2π-periodic functions, $x(\tau) = x(\tau + 2\pi)$, by Fourier polynomials (Fourier series, truncated after the N-th term):

$$x(\tau) = a_0 + \sum_1^N (a_n \cos n\tau + b_n \sin n\tau) = a_0 + \sum_1^N c_n \cos(n\tau + \varphi_n). \tag{A.2}$$

The assembled Fourier coefficients $(a_0, a_1, ..., a_N, b_1, ..., b_N)_x$ we denote by $\mathbf{f}_{cx}$. When x is a column vector, e.g. $x \Rightarrow \mathbf{u}$, the Fourier coefficients $\mathbf{f}_{cu}$ constitute a matrix. When we express the Fourier coefficients $\mathbf{f}_{cx'}$ of the derivative x' by those of x we write

$$(a_0, a_1, ..., a_N, b_1, ..., b_N)_{\dot{x}} = (0, 1\cdot b_1, ..., n\cdot b_n, ..., N\cdot b_N, -1\cdot a_1, ..., -n\cdot a_n, ..., -N\cdot a_N,)_x, \tag{A.3}$$

which we write in operator notation: $\mathbf{f}_{cx'} = \mathrm{d}\cdot\mathbf{f}_{cx}$; furthermore holds $\mathbf{f}_{cx''} = \mathrm{d}\cdot\mathbf{f}_{cx'} = \mathrm{d}\cdot(\mathrm{d}\cdot\mathbf{f}_{cx}) =: \mathrm{d}^2\cdot\mathbf{f}_{cx}$.
The operation of (numerical) Fourier Analysis we abbreviate by $\mathbf{f}_{cx} = \mathbf{A}^F\,x$, the Fourier Synthesis by $x = \mathbf{S}^F\,\mathbf{f}_{cx}$.

The calculation of 2π-periodic solutions $\mathbf{q}(\tau) = \mathbf{q}(\tau + 2\pi)$ of the differential equation (22) runs as follows (cf. Urabe 1965): We abbreviate (22) by $\mathbf{H}(\mathbf{q}'', \mathbf{q}', \mathbf{q}, \tau, \Omega, \varepsilon) = \mathbf{0}$. For a numerical set of coefficients $\mathbf{f}_{cq}$ we obtain from (A.2), (A.3) etc. $\tilde{\mathbf{H}}(\tau) := \mathbf{H}(\mathbf{S}^F\mathrm{d}^2\cdot\mathbf{f}_{cq}, \mathbf{S}^F\mathrm{d}\cdot\mathbf{f}_{cq}, \mathbf{S}^F\mathbf{f}_{cq}, \tau, \Omega, \varepsilon)$ which should vanish. The condition $\tilde{\mathbf{H}}(\tau) = \mathbf{0}$ is replaced by its Galerkin-projection $\mathbf{f}_{cH} := \mathbf{A}^F\,\tilde{\mathbf{H}}(\tau)$ and $\mathbf{f}_{cH} = \mathbf{0}$. This leads to the set of $2\cdot(2N+1)$ equations

$$\mathbf{f}_{cH}(\mathbf{f}_{cq}, \Omega, \varepsilon) = \mathbf{0} \tag{A.4}$$

which is solved iteratively by Newton's method. (The array operations of MATLAB apply very favourably.)

References

Brommundt, E.; Krämer, E.: Instability and self-excitation caused by a gear coupling in a simple rotor system. (2004) in preparation.

Czerny, L.: Stabilitäts- und Schwingungsverhalten elastisch gelagerter Motoren mit Bogenzahnkupplung. *VDI-Berichte*, Düsseldorf (1993), Vol. 1082, pp. 417 – 435.

Deuflhard, P.; Bornemann, F.: *Scientific Computing with Ordinary Differential Equations*. Springer, New York etc. (2002), 485 p.

Deuflhard, P.; Hohmann, A.: *Numerical Analysis in Modern Scientific Computing*. 2nd Ed. Springer, New York etc. (2003), 337 p.

Farkas, M.: *Periodic Motions*. Springer-Verlag, New York etc. (1994), 577 p.

Jordan, D. W.; Smith, P.: *Nonlinear Ordinary Differential Equations*; 2nd edit. Clarendon Press, Oxford (1987), 381 p.

Ioos, G.; Joseph, D. D.: *Elementary Stability and Bifurcation Theory*. Springer-Verlag, New York etc. (1980), 286 p.

Krämer, E.: *Dynamics of Rotors and Foundations*. Springer-Verlag, Berlin etc. (1993), 383 p.

Ku, C.-P.R.; Walton Jr., J.F.; Lund, J.W.: A theoretical approach to determine angular stiffness and damping coefficients of an axial spline coupling in high-speed rotating machinery. *14th Biennial Conference on Mechanical Vibration and Noise (1993)*, pp. 249 – 256.

Morton, P.G.: Aspects of Coulomb damping in rotors supported on hydrodynamic bearings. *Workshop on Rotordynamic Instability Problems in High-Performance Turbomachinery*, A&M University, College Station, Tex. (1982), Proceedings pp. 45 – 56.

Piotrowski, J.: *Shaft Alignment Handbook*; 2nd Edit., Marcel Dekker Inc, New York etc. (1995).

Shiraki, K., Umemura, S.: *On the vibrations of two-rotor system connected by gear couplings*. *Technical Review*, Mitsubishi Heavy Industries Ltd., Tokyo (Jan. 1970), pp. 22 – 33.

Urabe, M.: Galerkin's procedure for nonlinear periodic systems. *Arch. Rational Mech. Anal*. (1965), pp.120-152.

Yamauchi, S.; Someya, T.: Self-excited vibration of gas-turbine rotor with gear coupling. *14th International Congress on Combustion Engines (CIMAC)*, Helsinki (1981), pp. GT8-1 to GT8-28.

Address: Prof. em. Dr. Eberhard Brommundt. Institut für Dynamik und Schwingungen, Technische Universität Braunschweig, PF 3329, D-38023 Braunschweig (Germany).
e-mail: E.Brommundt@tu-bs.de